Front. Chem. China 2010, 5(3): 299–308
DOI 10.1007/s11458-010-0215-4

FEATURE ARTICLE

Biomineralization of sea urchin teeth

Yurong MA (✉) and Limin QI

Beijing National Laboratory for Molecular Sciences, State Key Laboratory for Structural Chemistry of Unstable and Stable Species, College of Chemistry, Peking University, Beijing 100871, China

The sea urchin tooth, which is composed almost entirely of Mg-enriched $CaCO_3$, is of particular interest as a model for the study of biomineralization process due to its amazing mechanical toughness and hardness. Our recent work on the formation process, the crystal composition and orientation, and the mechanical properties of sea urchin tooth are summarized in this paper. First, transmission electron microscopy images and electron diffraction patterns, as well as crystal overgrowth experiments, show that the highly convoluted primary plate-lamellar needle complex grows into a single crystal of calcite from a transient amorphous precursor phase in the sea urchin tooth. Amorphous calcium carbonate exists in the center of both the primary plates and the needles, even though the surfaces are already well crystallized. Second, X-ray photoelectron emission spectromicroscopy demonstrates that the needles, primary plates, and polycrystalline matrix crystals are all aligned. And there are two alternating crystal orientations in the stone part of the sea urchin tooth. Microbeam X-ray diffraction patterns further prove the existence of the two crystal orientations in sea urchin tooth. The *c* axes of calcite in the two oriented crystals are only a few degrees from each other. Third, the mechanical properties of sea urchin tooth grinding tip were studied by nanoindentation. The polycrystalline matrix has a higher elastic modulus and hardness than single crystalline needles and plates. It is proposed that the grinding capability of the tooth can be attributed to the small and uniform sizes of the polycrystalline crystals, their high Mg contents, and the two co-orientations of single crystals and polycrystalline structure. The improved understanding of the biomineralization process of sea urchin tooth and the relations between their structures and mechanical properties may shed light on the design of mechanical grinding and cutting tools with tunable properties.

Keywords sea urchin tooth, biomineralization, high Mg calcite, amorphous precursor, crystal orientation

1 Introduction

Biomineralization is the process by which living organisms secrete inorganic minerals in the form of skeletons, shells, teeth, bones, etc. [1–4]. The biomineralization processes in nature have produced a lot of delicate biominerals with complex morphologies in several hierarchical levels and may thus own superior optical, electric, magnetic, and mechanical properties. The ability of the sea urchin tooth to grind down limestone is one of the most amazing paradigms in the field of biomineralization since both the tooth and the rock are composed almost entirely of calcite. Sea urchin has been an important experimental model for over a century, and vertebrates share many specific features of embryonic development with sea urchin. There is a special issue on the sea urchin genome on *Science* in 2006 [5]. The impressive ability of sea urchin tooth is certainly related to the structure of the whole tooth and especially the organization of the materials that make up the mature end, that is, the grinding tip of the tooth. The sea urchin tooth has been investigated extensively in order to understand the unique structural

Received March 6, 2010; accepted June 13, 2010
E-mail: yurong.ma@pku.edu.cn

features that enable it to function so effectively as a grinding tool in the past 60 years [6–13]. The major structural elements of the sea urchin tooth are single crystalline primary plates and needles composed of low Mg calcite (5–13 mol% Mg) and Mg-enriched calcite (40–45 mol% Mg) polycrystalline matrix confined to the stone part of the tooth. The latter has higher hardness and elastic modulus and is located in its central part, which is right at the grinding tip [9]. The polycrystalline matrix calcite crystals are enriched with very high percent of Mg, and thus, they were referred to as "protodolomite" [14], even though the structure corresponds to disordered Mg calcite.

Generally, the investigation on the biomineralization of sea urchin teeth involves the roles of proteins played in the mineralization, the mineral deposition process during the mineralization, and the structural and mechanical characteristics of the teeth. Since the biomineralization process is strongly related to the proteins in the biominerals, Veis et al. have done a lot of work on the extraction, purification, and analysis of the proteins in the sea urchin tooth in the recent years [8,11,13,15]. Mann et al. identified 138 proteins in the matrix of tooth powder, which is the most comprehensive list of sea urchin tooth matrix proteins available at present [16]. Other than the studies on the proteins in the tooth, the mineralization process, and the structural analysis are also very important parts in the biomineralization of sea urchin tooth. It has been shown that the plates and needles in the sea urchin tooth are being all aligned such that a whole tooth behaves like a single crystal based on X-ray diffraction [7] or as two crystals with a small angular offset based on polarized light microscopy [6]. Many questions concerning the nucleation, the crystal growth, and the orientation of the different single crystal needles and plates in sea urchin tooth still remain. Moreover, it is appealing to reveal what features of the tooth contribute to its superior mechanical properties as self-sharpening grinding tool. In this paper, our recent investigations on the mineral deposition process [17], the crystal composition and orientation [18], and the relations between the structures and the mechanical properties [19] of sea urchin teeth are reviewed.

2 Mineral deposition process [17]

The length of the plumula stage in the tooth of the sea urchin *Paracentrotus lividus* is about 4 mm. The plumula stage is arbitrarily divided into three stages: I, II and III. The three stages are schematically shown in Scheme 1, together with the main skeletal elements of the tooth. The plumula stage I, has a

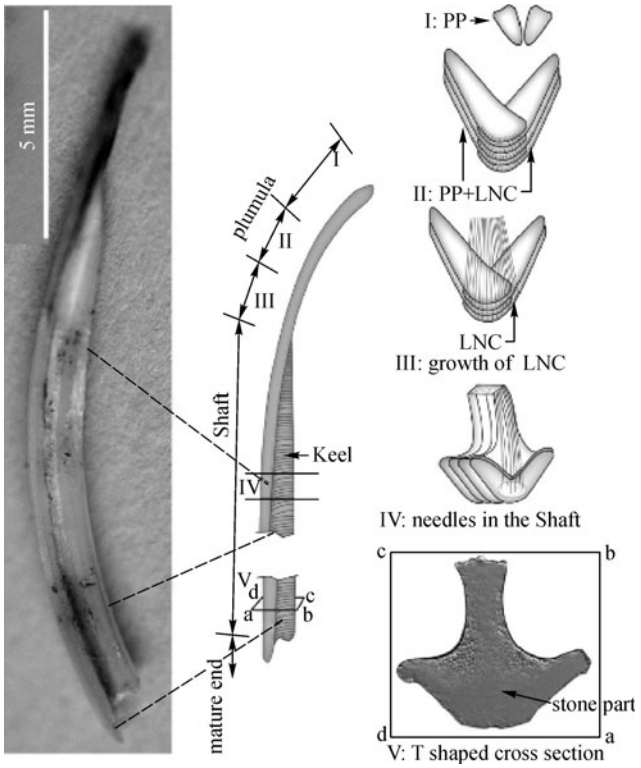

Scheme 1 Left: A whole tooth. Middle: Schematic representation of the stages of growth of the sea urchin tooth. Arrows show the direction of observation at different growth stages from the forming tip at the plumula stages (I, II, and III) to the Shaft (IV). Right: The stages of formation of the major skeletal elements that make up the plumula (stages I, II, and III) and keel in the shaft (stage IV). PP: primary plate; LNC: lamellar needle complex. Figure was reprinted with permission from Ref. [17].

length of about 2 mm. Plumula stages II and III are roughly 1 mm in length, respectively. At the macroscale, the needles and plates are remarkably well aligned. During development, a needle-plate complex forms a single crystal via an amorphous calcium carbonate (ACC) precursor phase.

The plumula of sea urchin tooth was immersed in 5% NaOCl for 30 min in order to remove the biomolecules on their surface and separate the tooth elements from each other. The lamellar-needle-complexes (LNCs) are attached to primary plates at the edge or the so-called basal net. The needles jut out from the primary plates at an angle. A primary plate (PP) with the connected LNCs from plumula I is shown in Figure 1(a) and (b).

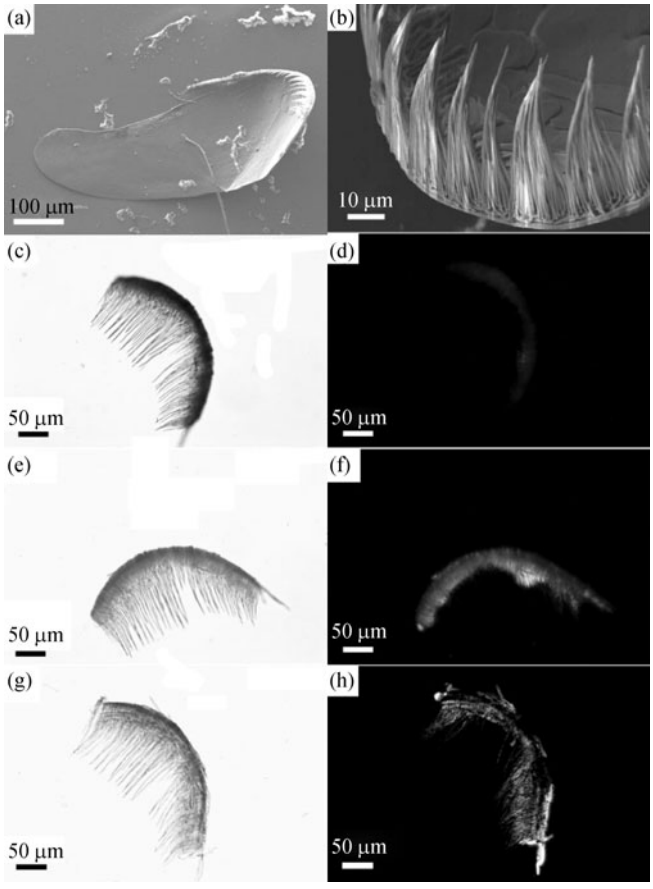

Figure 1 SEM and light microscopy images of sea urchin tooth elements from plumula stage I. (a) SEM image of a primary plate (PP) with attached lamellar needle complex (LNC). (b) SEM image of the LNC attached to the edge of the PP. (c), (e), (g) Light microscopy images of an LNC under plain light. (d), (f), (h) Light microscopy images of an LNC under polarized light. (c), (d) 30 min after extraction. (e), (f) After 7.5 h in water. (g), (h) After 48 h in water. Figure was reprinted with permission from Ref. [17].

A drop of aqueous suspension including freshly extracted tooth elements was transferred onto a glass slide and covered with a coverslip, and the borders were sealed with wax. LNCs separated from the primary plates were observed under polarized light microscopy. The whole LNC is about 300–400 μm in size and is composed of parallel needles with diameters of about 1 μm and a basal net (Figure 1(c), (e), (g)). The fresh LNC from plumula I is isotropic when rotating 360 degrees under polarized light (Figure 1(d)). This shows that this freshly extracted LNC is not crystalline. The same LNC became birefringent after maintaining in water for 7.5 h, indicating that it has partially transformed into a crystalline material (Figure 1(f)). After 48 h in water, most of the materials in both the basal net and the needles became birefringent and transformed into crystalline material (Figure 1(h)). The whole LNC shows uniform extinction at specific angles, which is consistent with single crystals. As only calcium carbonate is present in the LNC, except for the presence of a small amount of Mg and biomolecules [20], it was proposed that the amorphous material in the freshly extracted LNC is amorphous calcium carbonate (ACC) and that most of the ACC transformed into a single calcite crystal in water after 48 h. LNCs from plumula stage II are birefringent even when observed immediately after extraction and behave like single crystals. This indicates that both in vitro and in vivo ACC transforms into calcite in the lamellar needle complexes.

The sea urchin tooth behaves like two single calcite crystals [6,18,21]. This raises the question of whether all the plates and the needles attached to it are formed from only two nucleation events, or whether they are formed from many nucleation events, and then grow as two single crystals. To address this question, it is necessary to answer first whether a plate and the needles attached to it in each LNC has only one crystal orientation, which is hard to identify because of their curved surfaces. Crystal overgrowth was used to determine the crystallographic orientations of a plate and the needles that grow off the plate in one LNC from plumula II (Figure 2(a)–(c)). Newly grown calcite crystals nucleate epitaxially on the surface of the original calcite single crystals (needles and plates) through crystal overgrowth. The classical rhombohedral morphology of the overgrown calcite crystals provides information on the crystallographic orientation of the PPs and LNCs. It is shown from the SEM images that the overgrown calcite crystals on the PP and LNC are all aligned relative to each other (Figure 2(a)). The overgrown calcite crystals on the curved needles are also well aligned. The angle between the plate and the needles is ~ 63°. The c axis of calcite in the model is parallel to the edge of the PP.

The edge of the primary plate at the point where the LNC attaches to it was seen by tilting and rotating the sample holder under SEM (Figure 2(b)). The viewing angle in the model morphology is identified such that the crystal model orientation matches that of the overgrown crystals. It can be seen from Figure 2(b) that the needles are parallel to the [102]

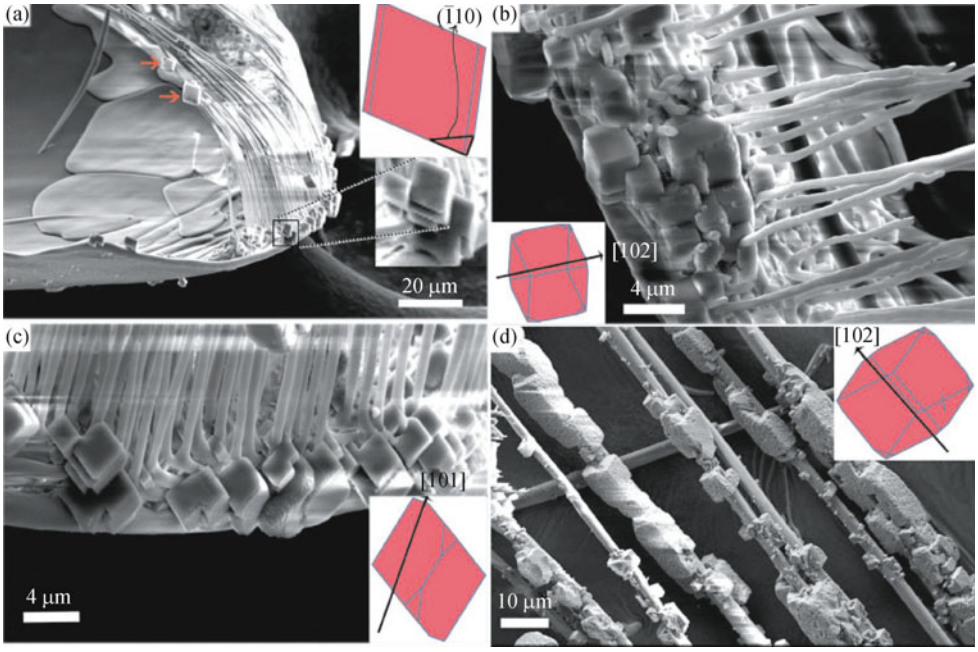

Figure 2 SEM images of overgrown calcite crystals on a primary plate (PP) and lamellar needle complex (LNC) from the plumula stage. Insets show the orientations of the overgrown calcite crystals simulated according to the observed morphologies. (a) PP and attached LNC from plumula stage II showing overgrown crystals on the needles and at the junction between the PP and LNC. (b) Higher magnification image, taken from a direction edge-on to the plate. (c) The same view as in (b), at a different location. (d) Overgrown calcite crystals on the needles from plumula stage III. Figure was reprinted with permission from Ref. [17].

direction of calcite in the model. Overgrown calcite crystals at another edge of the same PP (Figure 2(c)) are oriented parallel to the [101] direction of calcite. The angle between [102] and [101] is 12.7°. It can be seen that there is a small amount of variability in the orientation of the needles relative to the primary plate from the overgrowth experiments. The overgrown crystals on the needles are always parallel to those overgrown on the plate (Figure 2(a), (b)). Many overgrown calcite crystals can be seen at the base of the needles, but only a few crystals can be seen along the needles (see the red arrows in Figure 2(a)) because the needles at the plumula II stage are only partially transformed to calcite via ACC. A lot of well-oriented calcite crystals grew along the needles in the LNC from plumula III, which is also parallel to the [102] direction of calcite.

The crystal overgrowth experiments thus show that the PP and the attached LNCs essentially behave as a single calcite crystal in three dimensions even though the needle complexes are still growing, containing partially with calcite on the surface and amorphous calcium carbonate in the center of the needles. The PP and the needles attached to it have only one crystallographic orientation even though the PP and LNCs form at different times and have totally different morphologies, and all are enclosed in membranes [22–24].

It was demonstrated that the lamellar-needle complexes in the plumula of the sea urchin teeth form by the initial deposition of amorphous calcium carbonate, which subsequently transforms into the single crystal of calcite. The ability to grow a single crystal into such a complex shaped morphology is almost certainly due to the initial deposit as an amorphous phase. This is one feature of the tooth formation process that can be emulated in the fabrication of complex synthetic materials [25,26]. The fact that the sea urchins uses such structures in conjunction with a multicrystalline phase to produce a highly effective grinding tool demonstrates the functional utility of single crystals.

3 Structural characterization: crystal orientation and Mg mapping [18]

Although it is not clear whether each needle-plate complex nucleates independently or the complexes are all somehow connected in the tooth, it is remarkable that a whole tooth behaves as a single crystal based on X-ray diffraction [7] or as two crystals based on polarized light microscopy [6]. Therefore, more information is needed to address this dichotomy.

3.1 Crystal orientation

In this part, X-ray photoelectron emission spectromicroscopy (X-PEEM) and Microbeam X-ray diffraction patterns provide

structural, compositional, and orientational information with spatial resolutions at different length scales ranging from nanometers to tens of microns.

X-PEEM maps from the same area in the cross section of the tooth tip were shown in Figure 3(a)–(d). The needles (elliptical spots) and plates (stripes) in the tooth tip are both dark because they contain lower concentrations of Mg relative to the very high-Mg polycrystalline matrix (bright areas) in the Mg distribution map (Figure 3(a)). The needles and plates are brighter as they have higher Ca concentrations in the Ca distribution map of the same region (Figure 3(b)). The C and O polarization-dependent imaging contrast (PIC) maps (Figure 3(c) and (d)) were obtained by the digital ratio of X-PEEM micrographs, acquired at the π^* and σ^* peak energies for both carbon and oxygen. Note that the C and O concentrations are the same in the whole area of the stone part, as all the grinding tip of the tooth is composed of Ca/Mg carbonate. The different gray levels in the carbon and oxygen PIC maps are due to different crystal orientations relative to the polarization vector in the illuminating X-ray beam in alternating regions [27]. It is surprising that not only are the tooth plates and needles aligned within each of these regions

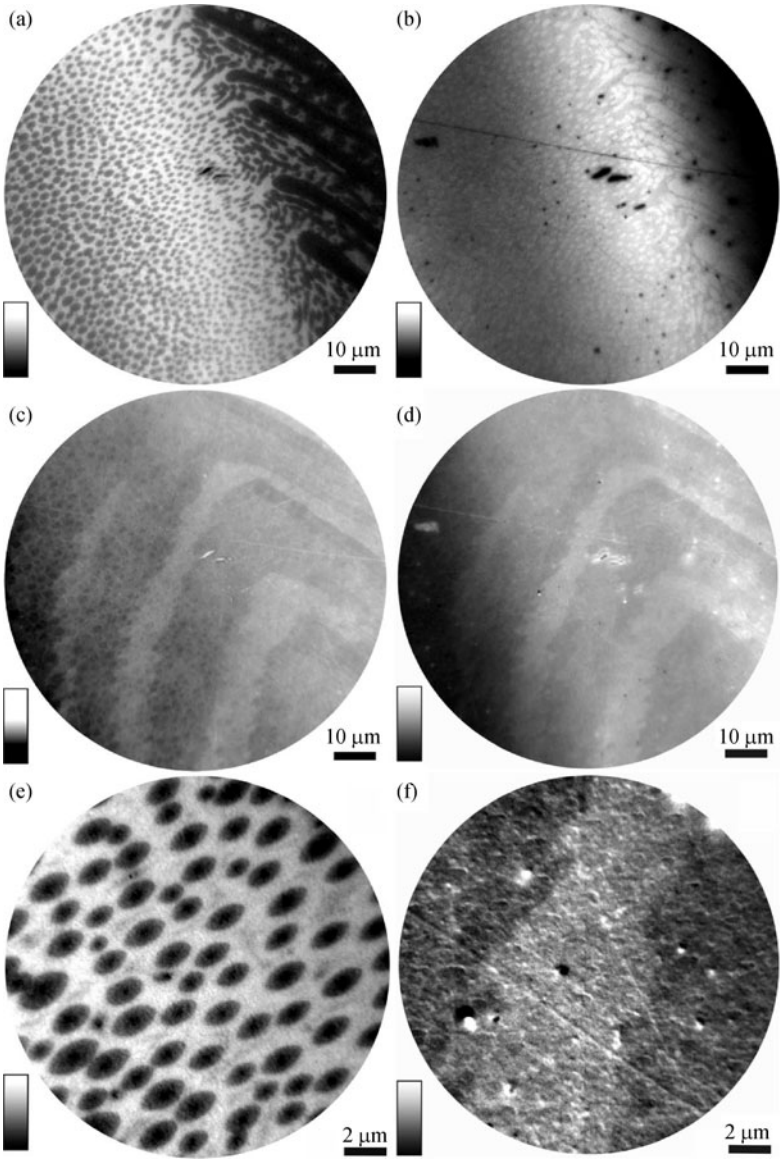

Figure 3 X-PEEM elemental maps of the stone part in the transverse cross section of the sea urchin tooth at the mature end, that is, the grinding tip of the tooth. (a), (b), and (e) show elemental concentrations of Mg, Ca, and Mg, respectively. (c), (d), and (f) are carbon and oxygen polarization-dependent imaging contrast (PIC) maps, displaying different crystal *c*-axis orientations with different gray levels. (a)–(d) are from the same area. (e), (f) are from a small region in the center of the area shown in (a)–(d). Figure was reprinted with permission from Ref. [18].

but also the polycrystalline matrix with very high Mg percent. The two gray levels in the C and O maps (Figure 3(c) and (d)) are attributed to rotations in the two *c*-axes of calcite [28]. The needles and the polycrystalline matrix surrounding them have almost the same gray level and thus have the same *c*-axis orientation (Figure 3(f)). The Mg map at the same region, as in Figure 3(f), is shown at the same magnification as a reference (Figure 3(e)). This is the first time to find the two locally oriented and alternating regions at such high resolution in the sea urchin tooth. However, a disadvantage of X-PEEM PIC maps is that they could not provide quantitative information on the c axes of the two crystal orientations nor on the angular difference between the two orientations.

Microbeam X-ray diffraction was applied to study the predominant orientations of calcite crystals in different regions of the sea urchin tooth. One transverse cross section with thickness about 100 μm was used to obtain diffraction patterns (Figure 4(a)), using a 10-μm wide beam. As an example, one quadrant of a 2D diffraction pattern obtained from the central region of the stone part was shown in Figure 4 (b), with an oscillation angle of ±90°. This "rotating crystal" diffraction pattern reveals essentially a single crystalline Mg-calcite pattern with a few degrees' azimuthal spread of the reflections. The vertical symmetry line of the cross section (corresponding to the rotation axis) is close to the [018] direction, and the calcite *c*-axis direction is tilted by ~ 15° from the vertical. The (104) reflections are investigated in more detail for several positions in Figure 4(c)–(e). Within the scanned region marked with green box in Figure 4(a), the (104) reflection always appears in the rotation interval between −5° to +10°, while 0° corresponds to the beam being perpendicular to the cross section. Two slightly different orientations can be seen in the pattern from the center of the tooth tip, as indicated by the presence of a double peak (Figure 4(d)). However, only one peak dominates on either side of the tooth stone part (Figure 4(c) and (e)). Similar observations were obtained for the entire upper region (60 μm from the top line of the green box in Figure 4(a)), where primary plates and polycrystalline matrix dominate. However, in the lower part of the box in Figure 4(a), where needles and polycrystalline matrix dominate, a slightly broader distribution and more than two azimuthal maxima were observed, which are generally consistent with the two main crystal orientations observed in the upper part. We note that the X-PEEM images in Figure 3 do show that the needles and polycrystalline matrix have two alternating *c*-axis orientations in the stone part of sea urchin tooth, a little different from the microdiffraction results. The diffraction patterns from the longitudinal sections also reveal essentially two single crystal Mg-calcite misoriented by about 0.6° azimuthal difference based on the [006] reflection. This indicates that in the grinding tip of the sea urchin tooth, the two *c*-axes are misoriented by less than about 6° if we take into account the oscillation angle of ±2.5°.

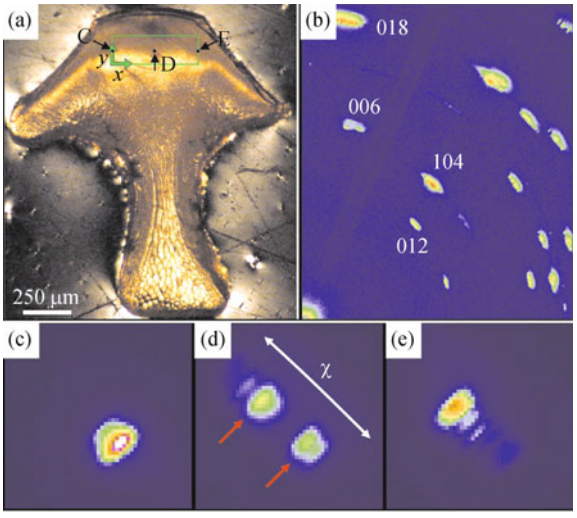

Figure 4 Microbeam X-ray diffraction from a transverse cross section in the stone part of the mature sea urchin tooth. (a) A polarized light micrograph of one typical specimen used for microbeam diffraction. (b) Rotating crystal pattern (oscillation angle ± 90°) from the center of the green box shown in (a). (c)–(e) Zoomed-in images of the (104) reflection of calcite obtained at positions indicated by arrows in (a). Figure was reprinted with permission from Ref. [18].

The high-resolution characterizations by using X-PEEM and Microbeam X-ray diffraction show that in the sea urchin tooth tip the needles, plates, and the high Mg polycrystalline matrix are all oriented. A region of co-oriented plates, needles, and the polycrystalline matrix was defined as a "block." Two differently oriented crystalline blocks are interdigitated in the tooth tip. A scheme was drawn to show the crystal orientations

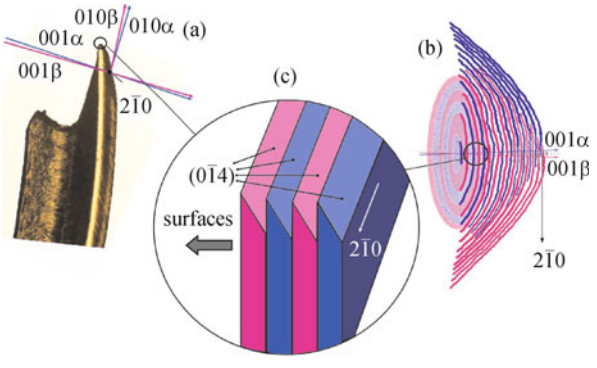

Scheme 2 Summary of crystallographic orientations of the calcite plates in the sea urchin tooth tip. (a) The approximate crystallographic orientations in relation in the tooth tip. (b) A schematic illustration of the crystal orientations in the transverse cross section of the sea urchin tooth at the grinding tip (viewed from the top). (c) An enlarged 3D schematic of the calcite plates in the tooth tip. Figure was reprinted with permission from Ref. [18].

of the calcite plates in the sea urchin tooth tip (Scheme 2) [18]. Each color represents a single crystal orientation, including co-oriented single crystalline plates, needles, and the polycrystalline matrix, collectively referred to as a crystalline "block." Magenta and blue blocks alternate. The calcite c-axes are separated by 1°–6° and are both tilted off-plane by about 15° from the vertical symmetry line (as shown in Scheme 2(a)). The two groups of primary plates are drawn in magenta and blue according to the SEM image of the transverse cross section of tooth (Scheme 2(b)). At the center, the plates from one side are always covered by plates from the other side. The polycrystalline matrix aligned with the blue set of plates and needles is shown in pale blue, and the matrix aligned with the magenta set of plates and needles is in pale magenta. The presence of two crystals is consistent with the proposal of Märkel that the whole tooth has basically two orientations based on polarized light microscope images [6,21,29].

It is shown that an individual plate-needle complex forms one single continuous crystal, despite its complex morphology [17]. However, it is not known how many of these plate-needle complexes are aligned. One possibility is that all the aligned components were actually only nucleated once and that they are all part of one structural continuum. As the tooth is composed of two such co-oriented complexes, this would imply two slightly differently oriented nucleation sites. The alignment of the nanosized crystals of the polycrystalline matrix with the needles and plates is puzzling. The alignment is less puzzling if one assumes a process of secondary nucleation, starting from the plates, which are not coated by a membrane but by a loose network of organic molecules. In this scenario, crystal orientation would propagate through the network and eventually include all nanocrystals in the polycrystalline matrix. Furthermore, the extent of alignment of the crystals in the polycrystalline matrix is not as good as the alignment of the needles and the plates. This may indicate that the polycrystalline matrix constituents obtain their alignment by the mechanism of oriented attachment [30] or by secondary nucleation upon contact.

3.2 Mapping of the Mg concentrations

Mg distribution maps from X-PEEM provide information on Mg concentrations to a depth of about 12 nm below the surface and at a high resolution (up to 20 nm) (Figure 3(a) and (e)) [18]. It is clear from Figure 3(a) and (e) that the Mg concentration is not uniform: the different gray levels show that the cores of the needles contain less Mg than their peripheries, and there are some low Mg zones within the polycrystalline matrix (Figure 3(e)). The microbeam X-ray diffraction results indicate that the Mg concentrations in the tooth tip are graded such that there is an overall increase in the Mg concentrations of both the needles and the polycrystalline matrix toward the center of the tip. The sea urchin tooth tip is clearly the product of exquisite control.

Both the X-PEEM and microdiffraction could only offer qualitative information on the Mg concentrations in sea urchin tooth. Fortunately, the nanoscale secondary ion mass spectrometer (NanoSIMS) ion probe provides quantitative information on Mg concentrations at a resolution lower than X-PEEM but much higher than the X-ray microdiffraction used in this work. The spatial resolution is around 100 nm and the probing depth of each scan is about 10 nm. An Mg/Ca map of a polished transverse cross section of the tooth grinding tip via NanoSIMS shows that the Mg concentration of the polycrystalline matrix is about 45 mol% of Mg, which is close to that of dolomite, in agreement with the microdiffraction imaging of the Mg concentration of the polycrystalline matrix. The Mg contents in the polycrystalline matrix are more than three times higher than those in the single crystalline needles and plates. Mg is distributed uniformly in the polycrystalline matrix, with areas of higher Mg contents being located at some distance from the needles. NanoSIMS shows that the cores of the needles have less Mg than their rims. These observations from NanoSIMS are consistent with the X-PEEM and microdiffraction results.

Secondary ion mass spectroscopy (SIMS) was applied to mature teeth of *Lytechinus variegatus* to map Ca, Mg, and amino acid fragments, such as Asp and Ser [11]. Aspartic acid was strongly colocalized with very high Mg content regions of the tooth (the stone part) (Figure 5) [11]. The left-most column in Figure 5 shows total ion (a) or Ca ((f) and (k)) maps. The location of maximum Asp content in Figure 5(c) qualitatively matches that of the very high Mg in the stone part, Figure 5(b). Note that the calcium distribution image appears structureless (Figure 5(f) and (k)). At higher magnification, the primary plates (Figure 5(f)–(j)) show precise modulation of Mg concentration between columns and plates and colocalization of Asp residues with very high Mg calcite (Figure 5(i)). The same colocalization is seen in Figure 5(n) (green pixels) where the very high magnesium calcite between needles correlates with aspartic acid residues below the stone part (area "B" in Figure 5(d)). Demineralized specimens showed reduced Mg and Asp signals, whereas Ser content had the same distribution in demineralized and mineralized sections, emphasizing the association of very high Mg calcite and readily soluble Asp-rich protein(s) [11].

4 Mechanical properties [19]

Sea urchins obtain their food by scraping rocky surfaces by using tooth composed almost entirely of magnesium-enriched

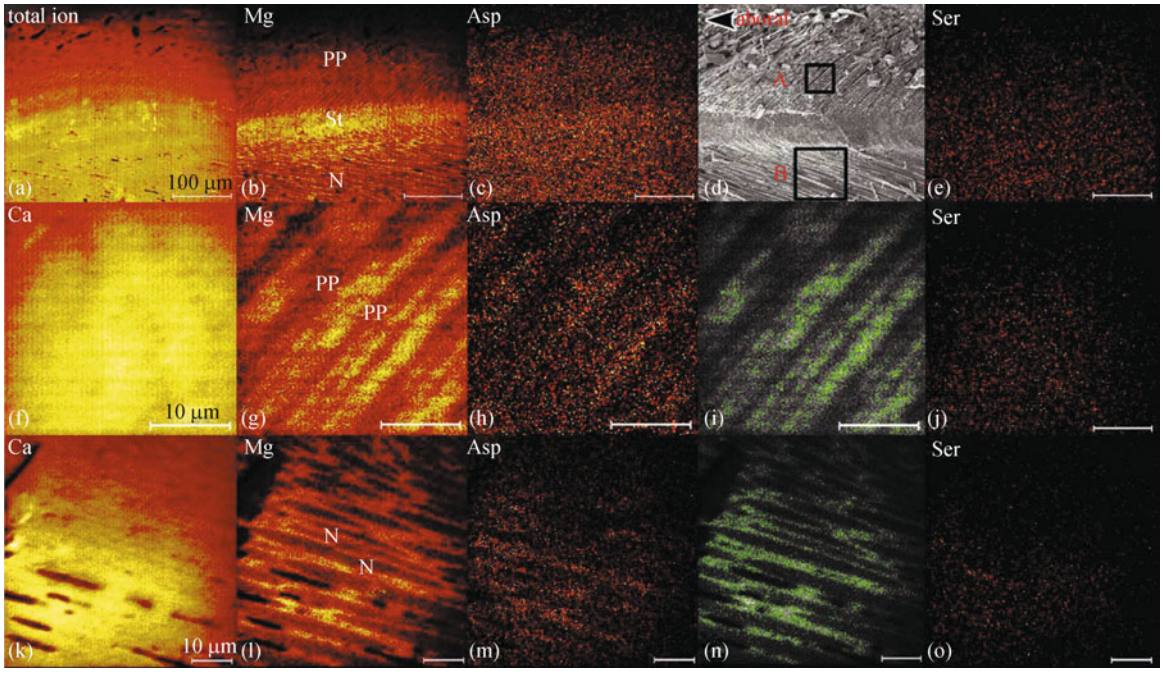

Figure 5 SIMS maps of longitudinal cross section of a sea urchin tooth through the flange, with primary plates (PP), stone part (St), and needles (N) labeled. Each row shows a maps of one area, the top row showing a low magnification overview and the middle and bottom rows showing higher magnification views of areas A and B, respectively. Figure was reprinted with permission from Ref. [11].

calcite. The key to the high mechanical properties lies in the unique structural attributes of the teeth. In this part, we investigated how the different kinds of calcite crystals in the sea urchin teeth work together as an effective grinding tool.

SEM studies indicate that the working face of the tooth tip of a sea urchin living on natural rocky substrates is covered with a smear layer, while the single crystal needles are barely visible [19]. This implies that the abrasion has preferentially removed more of the needles and plates as compared to the polycrystalline matrix. The smear layer presumably includes both the polycrystalline matrix and the abraded plates and needles.

Nanoindentation was used to characterize freshly polished cross sections of the sea urchin tooth at the mature end. Different situations, such as high Mg polycrystalline matrix, plates, needles, and the borders between the matrix and the needles were analyzed separately (Table 1). The E (borders) and H (borders) values are from indentations within a few hundred nanometers from the sharp visible boundary between polycrystalline matrix and needles or plates. Both the mean elastic modulus (E) and hardness (H) values of the high Mg calcite polycrystalline matrix are higher than the values obtained for pure synthetic calcite and the needles but lower than the values for geological dolomite obtained in our work. We note that the values of dolomite obtained by nanoindentation in Table 1 are higher than those in literatures [31,32]. It is

Table 1 Mechanical properties of mature sea urchin tooth determined by nanoindentation. E: Elastic modulus; H: Hardness; SD: standard deviation; n: the number of indentations

	mean (GPa)	SD		mean (GPa)	SD
E (polycrystalline matrix)	98.5 (n = 15)	15.2	H (polycrystalline matrix)	5.7 (n = 15)	1.1
E (borders)	79.5 (n = 15)	5.7	H (borders)	3.9 (n = 15)	0.4
E (needles)	71.1 (n = 7)	8.4	H (needles)	3.5 (n = 7)	0.9
E (plates)	76 (n = 7)	4.6	H (plates)	3.8 (n = 7)	0.4
E (calcite)	73.5(n = 11)	2.9	H (calcite)	2.7(n = 11)	0.23
E (dolomite)	117(n = 14)	7.8	H (dolomite)	6.5(n = 14)	0.86
E (dolomite)[a]	70		H (dolomite)[b]	3.9	

a) The E (dolomite) value is acquired from Ref. [31].
b) The H (dolomite) value is obtained from Vickers hardness of dolomite 420 kg·mm^{-2} from Ref. [32] multiplied by 92.65. Data were reprinted with kind permission from Ref. [19].

proposed that the values of geological dolomite obtained by nanoindentation reflect the single crystalline properties of dolomite. These values are more reasonable as a basis for comparison to the data presented here. The values for the borders between the Mg-enriched polycrystalline matrix and needles are similar to those of the needles and the plates.

The surface impressions after nanoindentation on the stone part of the mature sea urchin tooth were characterized by SEM (Figure 6) [19]. The cross sections of the needles are elliptical or round in these SEM images (Figure 6(a), (d)), whereas the cross sections of the plates are ribbon-like (Figure 6(b)). All the indentations from the polycrystalline matrix have no cracks (Figure 6(c)). In contrast, all the indentations from the single crystalline needles and plates have small cracks emanating from the corners of the indentations (Figure 6 (d)). This indicates that the polycrystalline matrix has higher fracture toughness relative to the single crystalline needles and plates, according to studies of ceramic toughness [33]. The unique properties of the matrix is probably due to a combination of a very high Mg content, the very small size of the nanocystals, and the lack of local orientation of the nanocrystals from TEM studies [19]. It is proposed that the organic macromolecules in the sea urchin teeth also contribute to the superior mechanical properties.

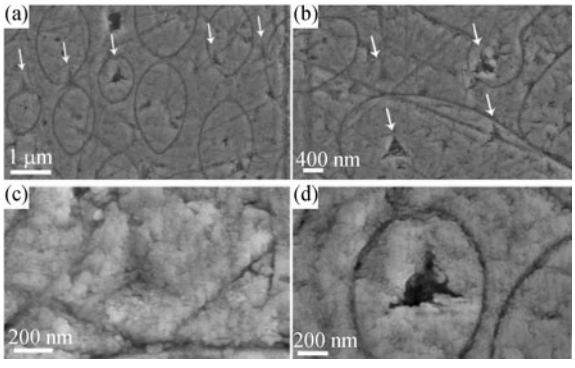

Figure 6 SEM images of the polished surface of the stone part of a sea urchin tooth after nanoindentation. (a), (b) Images showing the needles (oblique view in (a)) and plates (b) surrounded by the polycrystalline matrix (The linear striations are scratches). The arrows show the locations of the indentations; (c) Indentation on polycrystalline matrix; (d) Indentation on a single crystal needle. Figure was reprinted with permission from Ref. [19].

5 Conclusions

A deep understanding of the structural design features of the sea urchin tooth tip sheds light on the manner in which one crystalline phase, calcite, can be tailored to fulfill grinding and self-sharpening functions that enable the tooth to be used to grind holes into a substrate that is also composed only of calcite. The formation process, the crystal composition and orientation, and the mechanical properties of sea urchin tooth were summarized in this paper. First, calcite crystal overgrowth shows that the highly convoluted primary plate-lamellar needle complex grows into a single crystal of calcite using a transient amorphous precursor phase in the sea urchin tooth. Second, X-PEEM and Microbeam X-ray diffraction patterns demonstrate that the needles, primary plates, and polycrystalline matrix crystals are all aligned and that there are two alternating crystal orientations in the stone part of the sea urchin tooth. The *c* axes of calcite in the two oriented crystals are 1°–6° from each other. Last, the mechanical properties of sea urchin tooth grinding tip were studied by nanoindentation. The polycrystalline matrix has a higher elastic modulus and hardness than the single crystalline needles and plates. It is proposed that the grinding capability of the tooth can be attributed to the small and uniform sizes of the polycrystalline matrix crystals, their high Mg contents, and the two co-orientations of single crystals and polycrystalline structure.

The tooth of sea urchins are perhaps the pinnacle of materials design achievement in the echinoderms and much can be learned from them for the synthesis of functional materials. One thing is to synthesize single crystals via transient amorphous phase and to design well-aligned single crystals via secondary nucleation and oriented attachment. Another important conclusion from the nanoindentation of sea urchin tooth is the high modules and hardness of high Mg calcite polycrystalline matrix. It indicates that Mg-bearing calcite has better mechanical properties than pure calcite. Furthermore, organic macromolecules in the tooth also contribute to the superior mechanical properties of tooth and allow it to deform in a plastic manner and fracture with conchoidal cleavage. However, there are still many miracles for the biomineralization process of sea urchin tooth. For example, are there two or more nucleation events in the tooth? Why does the tooth suffer to align all the single crystalline needles and plates with two crystal orientations with only a few degrees from each other? How to realize the alignment of the high Mg calcite polycrystalline matrix with the single crystals in the circumference? All these questions related to sea urchin tooth and the inspiration from it for material science urge further investigations in this field in the future.

Acknowledgements Financial supports from the National Basic Research Program of China (Grant No. 2007CB815602) and the National Natural Science Foundation of China (Grant Nos. 50902002, 20873002, 20633010, and 50821061) are gratefully acknowledged.

Yurong MA studied food engineering and got her B.E. degree in 1998 from Shandong Institute of Light Industry. She got her M.E. degree in applied chemistry in 2001 from Jinan University, Shandong under the supervision of Prof. Xuelin Wang. She completed her Ph.D. study on physical chemistry–colloid chemistry under the supervision of Prof. Jiming Ma and Prof. Limin Qi from Peking University in 2004. She then went to the Max Planck Institute of Colloids and Interfaces, Germany to work with PD Dr. Helmut Cölfen and Prof. Markus Antonietti on non-classical crystallization processes of organic materials. Later on, she worked on biomineralization with Prof. Steve Weiner and Prof. Lia Addadi at the Weizmann Institute of Science, Israel. Now she is working as an associate professor on biomineralization and colloid chemistry at the College of Chemistry, Peking University.

References

1. Naka, K., *Biomineralization I (Kindle Edition)*; Springer, 2006
2. Naka, K., *Biomineralization II (Kindle Edition)*; Springer, 2006
3. Bäuerlein, E., *Handbook of Biomineralization: Biological Aspects and Structure Formation (vol. 1)*; Wiley-VCH, 2009
4. Cusack, M.; Freer, A., *Chem. Rev*. **2008**, *108*, 4433–4454
5. Special Issue on The Sea Urchin Genome, *Science* **2006**, *314*, 877–1032
6. Märkel, K.; Titschack, H. Z., *Morph. Tiere* **1969**, *64*, 179–200
7. Stock, S. R.; Barss, J.; Dahl, T.; Veis, A.; Almer, J. D., *J. Struct. Biol*. **2002**, *139*, 1–12
8. Stock, S. R.; Ignatiev, K. I.; Dahl, T.; Veis, A.; DeCarlo, F., *J. Struct. Biol*. **2003**, *144*, 282–300
9. Wang, R. Z.; Addadi, L.; Weiner, S., *Phil. Trans. R. Soc. B* **1997**, *352*, 469–480
10. Robach, J. S.; Stock, S. R.; Veis, A., *J. Struct. Biol*. **2005**, *151*, 18–29
11. Robach, J. S.; Stock, S. R.; Veis, A., *J. Struct. Biol*. **2006**, *155*, 87–95
12. Killian, C. E.; Metzler, R. A.; Gong, Y. U. T.; Olson, I. C.; Aizenberg, J.; Politi, Y.; Wilt, F. H.; Scholl, A.; et al., *J. Am. Chem. Soc*. **2009**, *131*, 18404–18409
13. Robach, J. S.; Stock, S. R., Veis, A., *J. Struct. Biol*. **2009**, *168*, 452–466
14. Schroeder, J. H.; Dwornik, E. J.; Papike, J. J., *Geol. Soc. Am. Bull*. **1969**, *80*, 1613–1616
15. Veis, A.; Barss, J.; Dahl, T.; Rahima, M.; Stock, S., *Microsc. Res. Techniq*. **2002**, *59*, 342–351
16. Mann, K.; Poustka, A. J.; Mann, M., *Proteome Sci*. **2008**, *6*, 11
17. Ma, Y. R.; Weiner, S.; Addadi, L., *Adv. Funct. Mater*. **2007**, *17*, 2693–2700
18. Ma, Y. R.; Aichmayer, B.; Paris, O.; Fratzl, P.; Meibom, A.; Metzler, R. A.; Politi, Y.; Addadi, L.; et al., *Proc. Nat. Acad. Sci. USA* **2009**, *106*, 6048–6053
19. Ma, Y. R.; Cohen, S.; Addadi, L.; Weiner, S., *Adv. Mater*. **2008**, *20*, 1555–1559
20. Weiner, S., *J. Exp. Zool*. **1985**, *234*, 7–15
21. Märkel, K., *Annot. Zool. Jpn*. **1970**, *43*, 188–199
22. Kniprath E Calcified Tissue Research, *Ultrastructure and Growth of Sea-Urchin Tooth* **1974**, *14*, 211–228
23. Märkel, K.; Röser, U.; Mackenstedt, U.; Klosterman, M., *Zoomorphology* **1986**, *106*, 232–243
24. Chen, C. P.; Lawrence, J. M., *Acta Zool*. **1986**, *67*, 33–41
25. Aizenberg, J.; Grazul, J. L.; Muller, D. A., Hamann, D. R., *Science* **2003**, *299*, 1205–1208
26. Li, C.; Qi, L. M., *Angew. Chem. Int. Ed*. **2008**, *47*, 2388–2393
27. Metzler, R. A.; Zhou, D.; Abrecht, M.; Chiou, J. W.; Guo, J. H.; Ariosa, D.; Coppersmith, S. N.; Gilbert, P., *Phys. Rev. B* **2008**, *77*, 064110
28. Gilbert, P.; Metzler, R. A.; Zhou, D.; Scholl, A.; Doran, A.; Young, A.; Kunz, M.; Tamura, N.; et al., *J. Am. Chem. Soc*. **2008**, *130*, 17519–17527
29. Märkel, K.; Gorny, P.; Abraham, K., *Fortschr. Zool* **1977**, *24*, 103–114
30. Xu, A. W.; Ma, Y. R.; Cölfen, H., *J. Mater. Chem*. **2007**, *17*, 415–449
31. Hatzor, Y. H.; Zur, A.; Mimran, Y., *Tectonophysics* **1997**, *281*, 141–161
32. Deelman, J. C., *Int. J. Earth Sci*. **1976**, *65*, 1055–1078
33. Ritchie, R. O., *Mat. Sci. Eng. A* **1988**, *103*, 15–28